



Effect of formic acid on aqueous corrosion mechanisms of mild steel

Sahithi Ayyagari, Maryam Eslami¹, Fazlollah Madani Sani, Yoon-Seok Choi, Bruce Brown, Srdjan Nestic*

Institute for Corrosion and Multiphase Technology, Department of Chemical and Biomolecular Engineering, Ohio University, Athens, OH 45701, United States

ARTICLE INFO

Keywords:

Corrosion
Formic acid
Acetic acid
Polarization
Mechanistic modeling

ABSTRACT

The effect of formic acid ($HCOOH$ or shortly HFr) on corrosion mechanisms of X65 steel was systematically investigated in pH controlled, N_2 -sparged and CO_2 -sparged solutions using potentiodynamic polarization and linear polarization resistance (LPR) techniques. The results from the electrochemical experiments conducted in 1 wt.% $NaCl$ solutions at 1 bar (total pressure) confirm that HFr is not significantly electroactive and therefore is not directly reduced on the steel surface under the conditions studied here. Experiments at various HFr concentration, temperature, pH, and flow rate also confirm that the main role of HFr on the corrosion of X65 steel is through the “buffering effect” mechanism. According to this mechanism, weak acids such as HFr increase the cathodic limiting current by providing hydrogen ions (H^+) through their chemical dissociation similarly as is seen with acetic acid (CH_3COOH or HAc).

A comparison between HFr and HAc shows that these two organic acids have some differences in their behavior. First, HAc seems to retard the anodic reaction and decrease the corrosion rate, especially at lower temperatures and higher concentrations, while HFr does not. Second, the influence of these two acids on increasing the limiting current density seems to be similar at 30 °C, but at higher temperatures (50 °C, 80 °C), the cathodic limiting current density in the presence of HAc is greater than that with HFr at the same molar concentration. Under similar experimental conditions, HAc was observed to be less corrosive at lower temperature (30 °C), and more corrosive at higher temperatures (50 °C and 80 °C) compared to HFr at the same molar concentration.

Experimental data collected in this study were used to validate a newly developed mechanistic model. According to our investigations this model shows an accurate fit to the experimental data at different HFr concentrations and pH at 30 °C. However, the model deviates from the experimental limiting current density value at higher temperatures (50 °C and 80 °C). It is speculated that this deviation results from a potential inaccuracy in the available temperature function for equilibrium constant of HFr dissociation reaction, which requires further investigations.

1. Introduction

Internal corrosion of oil and gas pipelines is attributed not only to the produced water saturated with acidic gases such as CO_2 and H_2S , but also due to the presence of low molecular weight organic acids most common of which are formic acid ($HCOOH$ or HFr), acetic acid (CH_3COOH or HAc), and propionic acid (CH_3CH_2COOH) [1]. Field data shows that these organic acids, and particularly HAc can significantly increase the corrosion rate of mild steel pipelines in saturated CO_2 and H_2S aqueous environments [2–5]. Hence most of the studies since were focused on elucidating the role of HAc in corrosion of mild steel and will

be reviewed here first. The electrochemical activity of HAc and its mechanistic role in acceleration of corrosion rate has been a contentious issue for a long time. Most research has been focused on whether HAc can be directly reduced on the metal surface in addition to acting as a buffer for hydrogen ion (H^+) concentration. Such importance has led into numerous studies on determining the fundamental role of HAc on the aqueous corrosion of mild steel.

These studies go back to 1984, when Hurlen et al. [6] presented cathodic polarization curves of iron electrodes in deoxygenated aqueous buffered HAc solutions at pH 4.7 and 9.5 with different HAc concentrations. At the time, the direct reduction of weak acids such as HAc was

* Corresponding author.

E-mail address: nesic@ohio.edu (S. Nestic).

¹ Present address: Illinois Applied Research Institute, Grainger College of Engineering, University of Illinois Urbana-Champaign, Champaign, IL 61820.

considered a fact. However, Hurlen *et al.*'s results [6] showed that *HAc* is probably not an electroactive species, and its sole role is to provide more hydrogen ions for the hydrogen reduction reaction, i.e. act as a buffer. Despite this observation, the direct reduction of *HAc* remained an accepted concept in many papers published since. Garsany *et al.* [7] showed an increase in the cathodic limiting current density associated with the increase in *HAc* concentration, flow rate, and temperature. With the assumption of direct reduction of *HAc*, they tried to explain the "double wave" seen in cathodic polarization curves. They postulated different mechanisms of *HAc* reduction at different potentials. Despite using the assumption about direct reduction of *HAc*, which was later proven to be wrong, they hinted that the direct reduction of *HAc* is not a foregone conclusion: "the electrode cannot distinguish proton and undissociated acetic acid because of the rapid dissociation of acetic acid at the surface [7]". This has led to further efforts in understanding the effect of *HAc* (and in general, weak acids) on aqueous corrosion of mild steel. Contrary to Garsany *et al.* [7], George *et al.* [8] developed an electrochemical model where *HAc* was considered solely as a source of hydrogen ions (acting as a buffer) and assumed that it was not involved in a separate cathodic reaction (i.e. no direct reduction of *HAc*). Its contribution was mathematically accounted for by simply adding *HAc* mass transfer limiting current density ($i_{lim(HAc)}$) to the mass transfer limiting current density for hydrogen ion reduction ($i_{lim(H^+)}$). This model matched well with the experimental polarization data at pH 4 with different *HAc* concentrations (10 to 1000 ppm), different flow rates (rotating cylinder electrode at 500, 1000 and 4000 rpm), and different temperatures (20 to 80 °C). George and Nescic's further experimental observations [9] complemented those of Garsany *et al.* [7] on the effect of concentration, pH, flow rate, and temperature on CO_2 corrosion in the presence of *HAc*. Similar experimental studies were subsequently performed by Okafor *et al.* [10] and Amri *et al.* [11]. In these studies, the effect of *HAc* on the cathodic limiting current was highlighted and no significant influence on the anodic reaction was reported.

Reinforcing the notion of no direct reduction of *HAc*, Tran *et al.* [12] also reported no change in the charge transfer region for experiments conducted on stainless steel substrate at various *HAc* concentrations (at a constant pH). This indicated that, besides the reduction of hydrogen ions, there were no other significant cathodic reactions occurring at the metal surface. In other words, the direct reduction of *HAc* does not occur and *HAc* acts mainly as a buffer, i.e. a source of hydrogen ions, which can be observed as an increase in the limiting current for hydrogen reduction in experiments at a constant bulk solution pH. The studies by Kahyarian *et al.* [13,14] conducted with mild steel, also confirmed the "buffering effect" mechanism. Kahyarian *et al.* [14] developed a mathematical model based on the "buffering effect" that was effective in fitting the experimental data. An interesting observation from their study that needs highlighting, was the decrease in the anodic current density with the increase in *HAc* concentration at 30 °C, something that was also noted previously by George *et al.* [8] and other authors [15–17]. They speculated that *HAc* slightly retards the iron dissolution reaction due to adsorption on the metal surface.

As seen from this brief literature review, the existing literature predominantly concentrates on *HAc*, due to its prevalence in oil and gas production streams, and very little attention was paid to the effect of other water-soluble organic acids such as formic acid, *HFr*. Mostly because it was often assumed that the two acids (acetic and formic) behave similarly, the equilibrium dissociation constant (K_a) of *HFr* is higher by one order of magnitude compared to *HAc*, what suggests that it should not be simply assumed to behave the same as *HAc* and that there is a need to separately investigate the impact of *HFr* on corrosion of steel [18,19]. The research by Singh and Gupta [20,21] on the corrosion behavior of mild steel in concentrated aqueous solutions of formic acid showed an increase in the LPR corrosion rate by increasing the *HFr* content from 5 vol.% to 20 vol.%, but also a decrease in corrosion rate with further increase in the *HFr* content up to 80 vol.%. In addition, an

increase in the corrosion rate with increase in temperature (from 25 to 45°C) was reported regardless of *HFr* content. The authors explained their observations by considering the change in speciation ($HCOO^-$ and H^+ concentrations) with the concentration of *HFr* and temperature. However, with the use of an unbuffered solution and such high corrosion rates (> 10 mm/yr), the solution pH would have quickly increased due to the buildup in ferrous ion concentration ($[Fe^{2+}]$), which would cause a drastic change in aqueous speciation. Furthermore, the experiments were done in solutions with no control of flow and dissolved oxygen content. Their discussion was only supported by solution conductivity measurements, which makes their conclusions questionable. Similar experiments by Singh *et al.* with different mixture fractions of *HFr* and *HAc* (*HFr* : *HAc* (20:0, 19:1, 18:2, 15:5, and 10:10)) showed higher corrosion rate with higher *HFr* fraction [22]. However, lack of pH measurement (or pH control) in this study as well means that the increase in corrosion rate with the increase in *HFr* fraction could have been simply because the bulk solution was more acidic (had a lower pH). Although the information seems compelling to use, the lack of control over the water-chemistry means more than one parameter was varied in each set of experiments in most of the available studies. As a result, using the data from these experiments to develop a mechanistic model would be challenging. A more recent study by Eslami *et al.* [23] showed the influence of *HFr* on increasing the corrosion rate of steel at high temperature as well. As a result of these experiments with precise control of pH, authors have suggested that the formation of ferrous complexes in the presence of formate can compromise the formation and protective-ness of corrosion product layer (Fe_3O_4) leading to an increase in corrosion rate.

To the best of our knowledge, the only mechanistic corrosion study on the effect of *HFr* was conducted by Fajardo *et al.* in 2007 [24]. In this study, they also compared the behavior of other organic acids (carbonic acid, propionic acid, and acetic acid) to that of *HFr*. The electrochemical behavior of different organic acids was reported to be similar under the conditions of same pH and concentration of undissociated organic acids. Given that the concentrations of undissociated organic acids were calculated in ppm and since the studied acids have different molecular weights, their concentrations in molarity (M) would have been different which could lead to a faulty interpretation of the data. The authors attributed the increase in the corrosion rate by *HFr* to an extra cathodic reaction, the direct reduction of undissociated *HFr*, which was found to be dependent on temperature and controlled by diffusion, however, no direct evidence for the existence of this reaction was presented.

Considering the lack of systematic studies on the effect of *HFr* on CO_2 corrosion, the current paper presents a mechanistic study attempting to clarify the effect of *HFr* on corrosion mechanisms of mild steel. Precisely controlled polarization experiments using a rotating disk electrode (RDE) configuration were conducted to investigate the role of *HFr* under varying conditions of *HFr* concentration, pH, temperature, and flow rate. A few additional experiments were conducted to directly compare the electrochemical behavior of *HFr* and *HAc*. These experiments were conducted in N_2 -sparged deoxygenated solutions at a constant pH to study the effect of organic acids individually. Additional experiments were conducted in CO_2 -sparged solutions to more closely represent the field-like conditions. The obtained data (in N_2 -sparged solution at a constant pH) were also used to validate a recently developed mechanistic model [25].

2. Experimental

A typical three-electrode setup in a 2 L glass cell was used for the experimentation. In this setup, specimens of X65 mild steel, with a nominal chemical composition of C 0.14 wt.%, Si 0.25 wt.%, Mn 1.18 wt.%, P 0.012 wt.%, S 0.003 wt.%, Al 0.033 wt.%, Cr 0.15 wt.%, Mo 0.16 wt.%, Nb 0.027 wt.%, and Fe balance, were used as the working electrode (WE). In order to make an RDE configuration, an X65 disc spec-

imen with 5 mm diameter was press-fit into a Teflon holder. A platinum mesh served as the counter electrode (CE) and a saturated silver/silver chloride ($Ag/AgCl$ [KCl sat]) electrode was used as the reference electrode (RE). The temperature of the solution was controlled using a thermocouple and a controller linked to a hot plate/stirrer. The temperature was maintained with a maximum deviation of ± 2 °C with respect to the desired value. To prevent solution evaporation, especially at elevated temperatures, a condenser column was employed during the experiments. This effectively mitigated the loss of solution and maintained the desired solution composition. The details of the experimental setup are shown in Fig. 1.

For each measurement, the glass cell was filled with 2 L of a 1 wt.% (0.17 M) $NaCl$ solution. This solution was used since it provides high enough conductivity for electrochemical measurement. In addition, at 1 wt% the $NaCl$ concentration is not too high to affect the electrochemical behavior and lead to misinterpretation of the effect of the weak acids. A sparge gas, either N_2 or CO_2 was continuously bubbled through the electrolyte for approximately 2 h before and also during the experiment to maintain deoxygenation. Deoxygenated 1 M hydrochloric acid (HCl) or 1 M sodium hydroxide ($NaOH$) was added to adjust the pH at the beginning of the experiment. All the chemicals and gases used in this study were of analytical purity.

Before each polarization experiment, the rotating disk electrode (RDE) assembly shown in Fig. 1 was wet polished using 600, 800, 1000 and 1200 grit SiC emery papers, followed by successive diamond polishing using 9, 3, and 0.25 μm diamond suspensions. The RDE assembly was then rinsed with deionized (DI) water and isopropyl alcohol, loaded onto the RDE shaft, and immediately immersed into the electrolyte. After the initial stabilization of open circuit potential (OCP) for 20 min after which the change in OCP value was less than ± 1 mV, an electrochemical cleaning procedure was performed by applying anodic current density of $+5$ A/m^2 for 60 s, and then a cathodic current density of -5 A/m^2 for 60 s, followed by 120 s at the OCP. Then the same three steps were repeated for ± 2 A/m^2 and ± 1 A/m^2 . The cleaning procedure was

undertaken to guarantee a pristine electrode surface, completely free from any possible traces of iron oxide that may have formed during the specimen preparation. The cathodic steps favor the reduction of the iron oxide layer to ferrous ions and the anodic steps minimize the adsorption of hydrogen atoms that may be produced during the cathodic steps. This procedure ensured the repeatability of results [26]. After the electrochemical cleaning step, OCP was monitored for 20 min until a stable value was obtained, with short-lived potential fluctuations being less than ± 1 mV. This was followed by subsequently performing: cathodic polarization, electrochemical impedance spectroscopy (EIS), linear polarization resistance (LPR), and anodic polarization. In each experiment, the system was allowed to return to the OCP and stabilize before going to the next step.

LPR measurements were conducted by polarizing the WE from -5 mV to $+5$ mV with respect to OCP at a scan rate of 0.125 mV/s. The EIS measurements were performed to measure the solution resistance by applying an AC potential of 10 mV rms at OCP in a frequency range of 10 kHz to 0.1 Hz. After EIS and prior to each polarization experiment, OCP was monitored for an additional period of 1 min to assure the accuracy of the measurement. Cathodic and anodic potentiodynamic polarization sweeps were conducted from 0 to -0.55 V and from 0 to $+0.15$ V vs. OCP, respectively, at a scan rate of 0.5 mV/s. The polarization sweeps and the polarization resistance values reported here were corrected for the solution resistance effect obtained from EIS measurements. Corrosion rates were calculated using polarization resistance (R_p) obtained from LPR, solution resistance (R_s) obtained from EIS measurements, and B values of 13.2 mV/dec for tests conducted at 30 °C, 14 mV/dec at 50 °C, and 15.5 mV/dec at 80 °C.

Two sets of experiments were done in HFr and HAc solutions to investigate the effects of these organic acids on corrosion mechanism of mild steel. Each experiment was repeated twice. Table 1 provides the

details of these experiments. $K_{HFr} = 10^{57.528 - \left(\frac{2773.9}{T}\right) - 9.1232 \ln T}$

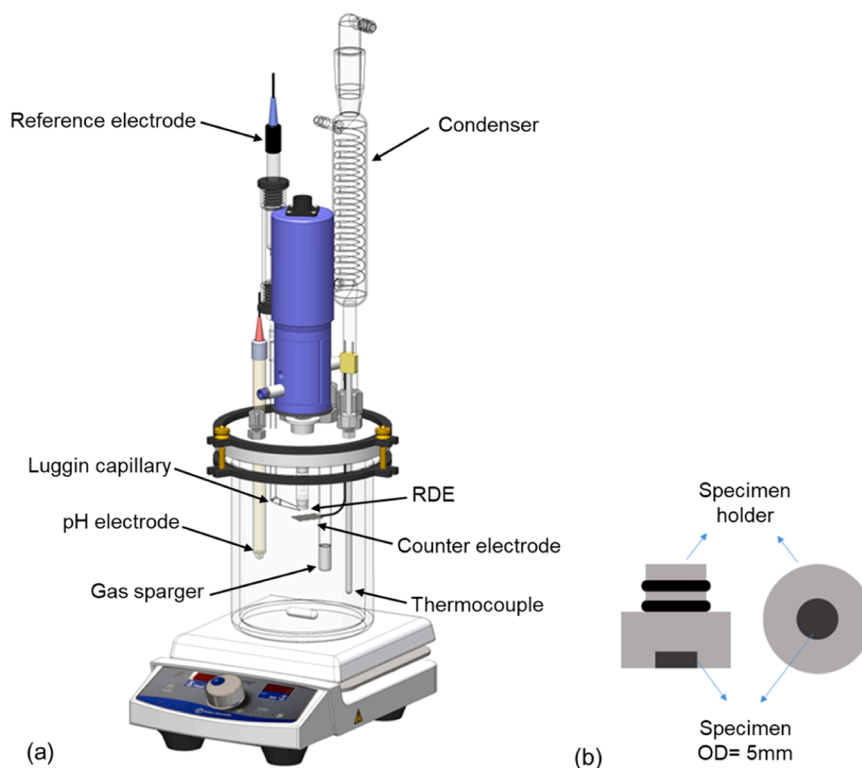


Fig. 1. Image of (a) glass cell setup with RDE (Image credit: Cody Shafer, Institute for Corrosion and Multiphase Technology), (b) 5 mm disk electrode press fit into a Teflon holder.

Table 1
Experimental conditions for the electrochemical measurements.

Experimental variable	Description	
	HFr (Exp. set 1)	HAc (Exp. set 2)
Undissociated acid concentration	0.14, 1.41, 14.18 mM (6.52, 65.26, 652.62 ppm)	0.14, 1.41, 14.18 mM (8.51, 85.19, 851.94 ppm)
Sparging gas	CO ₂ , N ₂	N ₂
pH	4, 5, and 6 (± 0.02)	4 (± 0.02)
Rotation velocity	1000, 2000, and 4000 rpm	2000 rpm
Test solution	1 wt.% NaCl	
WE material	X65 steel RDE	
Total pressure	1 bar (atmospheric pressure)	
Temperature	30, 50, and 80 °C (± 2)	

and $K_{HAc} = 10^{\left(\frac{-1500.65}{T} - 6.50923\log T - 0.0076792T + 18.67257\right)}$ (T in K) were used to calculate the acid concentrations in this table can be found in [18,19].

3. Results and discussion

3.1. Effect of formic acid on corrosion of mild steel

3.1.1. Effect of concentration

The effect of undissociated HFr concentration on polarization behavior of an X65 electrode at pH 4, 2000 rpm, and 30 °C is depicted in Fig. 2. The total HFr concentration ($c_{HCOOH} + c_{COOH^-}$) added to the solution was varied to achieve a constant concentration of undissociated HFr in the solution, set to 0.14, 1.41, and 14.18 mM in different experiments. The total HFr concentration was calculated using the Henderson-Hasselbalch equation shown below (Eq. (1)), which gives the relationship between the pH, pK_a, and the ratio of the concentration of HFr (HCOOH) to its conjugate base COOH⁻ in a solution.

$$pH = pK_a + \log\left(\frac{c_{COOH^-}}{c_{HCOOH}}\right) \quad (1)$$

The first observation made from Fig. 2 is that the limiting current density for the hydrogen reduction reaction increases with an increase in

concentration of undissociated HFr. As stated in the experimental conditions, the solution in all experiments was set to pH 4 and was held constant, hence the mass transfer limiting current density was the same in all these experiments. However, as the concentration of H⁺ decreased, the undissociated HFr in the solution readily dissociated to provide additional H⁺ for the reduction reaction. This is the definition of the “buffering effect” mechanism that leads to the increase in the limiting current density [14], and was progressively more pronounced as the concentration of undissociated HFr increased. The Tafel slope for the charge transfer portion, which is clearly visible as the straight section of the cathodic sweep for 14.1 mM HFr (yellow curve) does not show a significant deviation compared to those obtained with 1.41 mM, 0.141 mM, and 0 mM free HFr. This suggests that HFr does not directly participate in the reduction reaction, and that the charge transfer portion of the cathodic sweeps solely corresponds to the H⁺ reduction reaction. Therefore, it can be concluded that the charge transfer cathodic current densities for hydrogen evolution reaction are not affected by HFr concentration.

The anodic polarization curves in Fig. 2 show comparable behavior for the different concentrations of HFr. The curves in the active dissolution range, close to the open circuit potential, overlap within the error of measurement. This means that the presence and the concentration of HFr has no considerable influence on the active anodic dissolution of mild steel, under these conditions.

The associated corrosion rates obtained by using LPR are shown in Fig. 3. A relatively small increase in corrosion rate is observed with the concentration of undissociated HFr, particularly at lower HFr concentrations. This is primarily related to the increase in the limiting current density due to the “buffering effect”. In the absence of HFr, the corrosion was under mixed charge-transfer/limiting-current control (for H⁺ reduction). As the limiting current density initially increased with HFr concentrations (between the 0 and 1.41 mM) due to buffering, so did the corrosion rate. Eventually at higher HFr concentrations (>1.41 mM), the corrosion rate became predominantly controlled by charge transfer and the effect of buffering by HFr became much less significant.

3.1.2. Effect of flow rate

Fig. 4 shows the effect of flow on polarization behavior of X65 electrode at pH 4, 30 °C and in the presence of 1.41 mM of undissociated HFr. The potentiodynamic sweeps shown in this figure clearly indicate

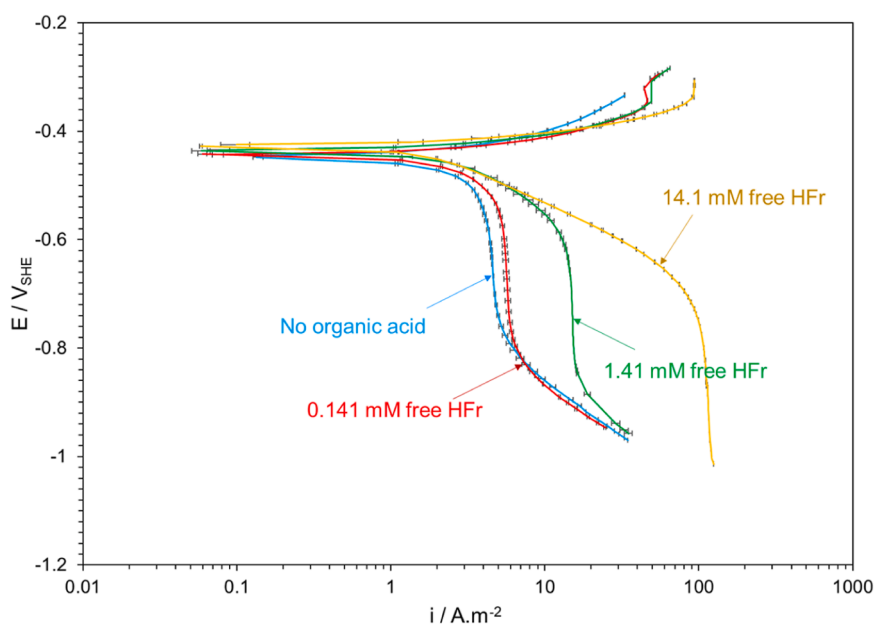


Fig. 2. Polarization behavior of X65 steel in N₂-sparged 1 wt.% NaCl solution at 30 °C, pH 4, 2000 rpm RDE, and various undissociated HFr concentrations (error bars show minimum and maximum values of current density at each potential).

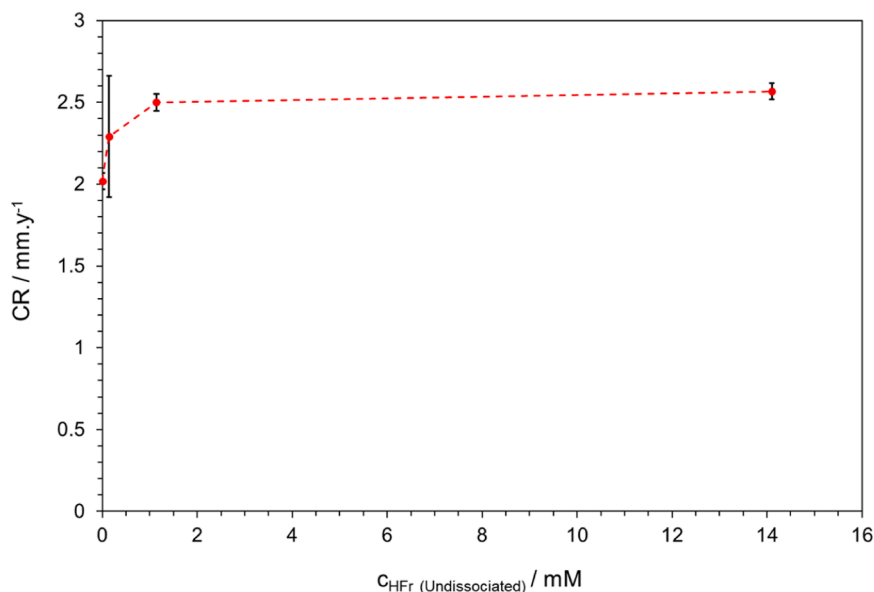


Fig. 3. Corrosion rates of X65 steel in N_2 -sparged 1 wt.% NaCl solution at 30 °C, pH 4, 2000 rpm RDE, and various undissociated HFr concentrations (error bars show minimum and maximum values of corrosion rate at each concentration).

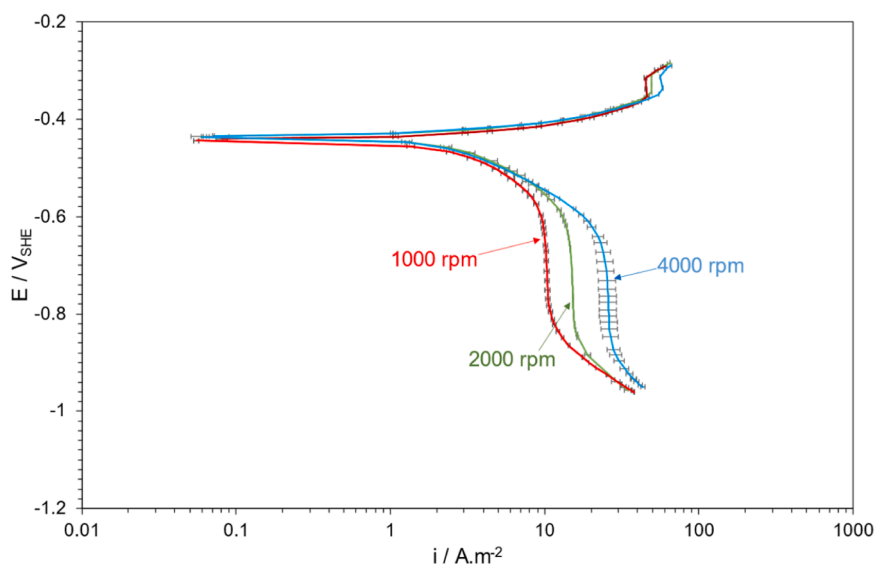


Fig. 4. Polarization behavior of X65 steel in N_2 -sparged 1 wt.% NaCl solution at 1.41 mM undissociated HFr , 30 °C, pH 4, and various flow rates (error bars show minimum and maximum values of current density at each potential).

the influence of rotation speed on the cathodic limiting current density, due to increased mass transfer of H^+ ions to the steel surface. This is consistent with the Levich equation [27] which directly correlates the mass transfer limiting current to the flow rate (rotational speed) for laminar RDE flow. The anodic reaction rate for iron dissolution was not affected by flow, as expected.

The corrosion rate shown in Fig. 5 was not changed much by the variation of flow rate. This further confirms that the corrosion process under these experimental conditions is predominantly controlled by the charge transfer rate for both H^+ reduction and iron dissolution with a minor effect of the limiting current density.

3.1.3. Effect of temperature

Temperature affects water speciation, and this needs to be accounted for first when analyzing the high temperature experiments. The equilibrium for chemical dissociation of HFr :



with the dissociation constant:

$$K_{HFr} = \frac{k_{f,HFr}}{k_{b,HFr}} = \frac{c_{H^+} \cdot c_{COOH^-}}{c_{HCOOH}} \quad (3)$$

changes with temperature as follows [18]:

$$K_{HFr} = 10 \left(\frac{57.528 - \frac{2773.9}{T_K} - 9.1232 \ln T_K}{T_K} \right) \quad (4)$$

In reaction (2), $k_{f,HFr}$ and $k_{b,HFr}$ are the reaction rate constants in forward and backward directions, respectively. In Eqs. (3) and (4) and, K_{HFr} is the equilibrium constant for HFr dissociation reaction, shown as a

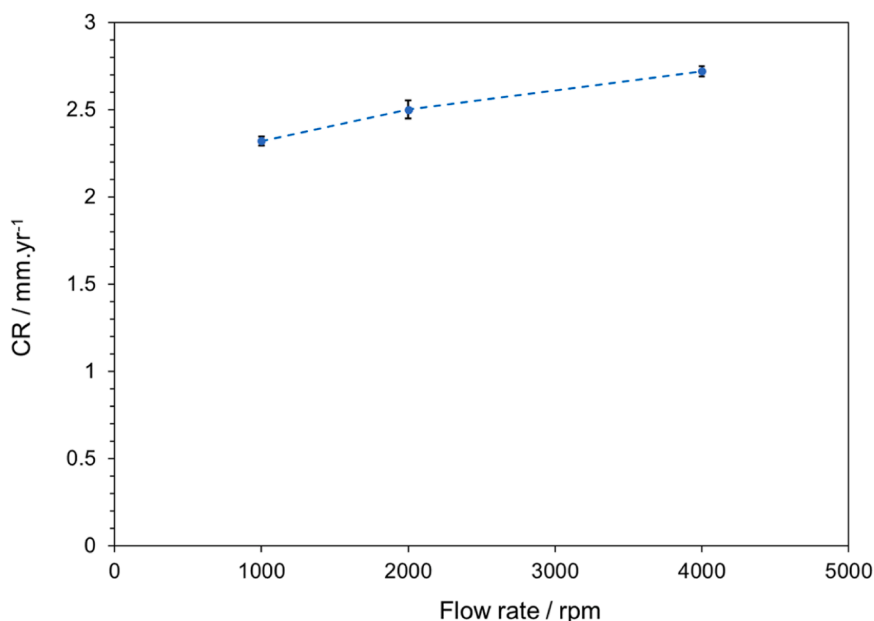


Fig. 5. Corrosion rates of X65 steel in N_2 -sparged 1 wt% NaCl solution at 1.41 mM undissociated HFr, 30 °C, pH 4, and various flow rates (error bars show minimum and maximum values of corrosion rate at each flow rate).

function of temperature, where T_K is the temperature in K.

Therefore, when pH (i.e. c_{H^+}) is kept constant, the change in temperature will alter the ratio between the undissociated formic acid (c_{HFr}) and formate ions (c_{COOH^-}), which needs to be accounted for in the high temperature experiments. In the current experimental design, the concentration of undissociated HFr was kept constant from experiment to experiment, by changing the total HFr concentration ($c_{HCOOH} + c_{COOH^-}$) accordingly. Therefore, the results in Fig. 6 isolate the effect of temperature on the polarization behavior at constant $c_{HFr} = 1.41$ mM and constant pH4, for a X65 RDE electrode rotating 2000 rpm. According to these potentiodynamic sweeps, the current densities for both anodic and cathodic reactions (in the charge transfer and limiting current controlled regions) increase with temperature, as would be expected. The change of rate for the charge transfer controlled parts of both cathodic and anodic polarization curves can be explained by Arrhenius law, which defines

the dependence between temperature and reaction rates [14], as will be shown below.

The effect on the limiting current density is somewhat more complex as the increase in temperature leads to a decrease in the density and viscosity of the electrolyte, faster HFr dissociation rates, higher diffusivity of the species involved in the reactions, which, on aggregate, lead to a higher rate of mass transfer of the species to the metal surface, and an overall increase in the cathodic limiting current density.

Due to the increase in temperature, the controlling reaction mechanism changes from being predominantly charge transfer controlled at lower temperature to predominantly limiting current controlled at higher temperature. This is because the charge transfer reactions are more responsive to a change in temperature than is the limiting current density.

Overall, the increase in the reaction rates with temperature leads to a

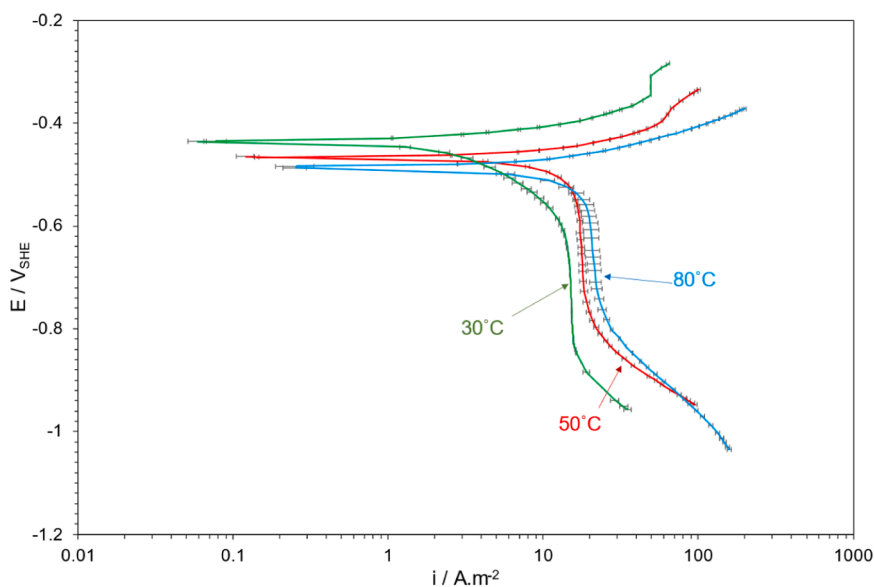


Fig. 6. Polarization behavior of X65 steel in N_2 -sparged 1 wt% NaCl solution at 1.41 mM undissociated HFr, 2000 rpm RDE, pH 4, at various temperatures (error bars show minimum and maximum values of current density at each potential).

pronounced increase in the corrosion rates as shown in Fig. 7.

3.1.4. Effect of pH

Fig. 8 shows the effect of solution pH on the polarization behavior of X65 electrode at 2000 rpm, 30 °C, at $c_{HFr} = 1.41$ mM. The ratio between the undissociated formic acid (c_{HFr}) and formate ions (c_{COOH^-}) is affected by the change in solution pH, as per Henderson-Hasselbalch Eq. (1), therefore from experiment to experiment done at different pH, the $c_{HFr} = 1.41$ mM was kept constant by adjusting the total HFr concentration ($c_{HCOOH} + c_{COOH^-}$) accordingly. Consequently, the extent of buffering induced by the HFr remains the same, despite varying the bulk solution pH from 4 to 6.

According to the results in Fig. 8, the decrease in c_{H^+} with an increase in pH has a strong influence on both the anodic and cathodic reactions. The charge transfer and limiting current densities of the cathodic polarization sweeps are directly affected by a change in pH and are the main cause for the decrease in the corrosion rate with pH, as depicted in Fig. 9. The charge transfer rate of the anodic reactions accelerates with an increase in pH, as the OH^- ion concentration increases, which contributes to the active dissolution of iron by forming catalytic iron hydroxide complexes [28]. In addition, with the pH increase, a transition from the active dissolution of iron to pre-passivation shifts to lower current densities, the same as was previously reported by Kahyarian et al. [29] for the case of HAc . Yet, these changes of the rate of anodic reaction have a significantly smaller effect on the corrosion rate, which is predominantly affected by the retardation of the cathodic reaction.

3.2. Effect of formic acid on CO_2 corrosion of mild steel

The role of HFr in CO_2 corrosion of mild steel was also investigated, as in practical applications, the two most often appear together. Additional experiments were done in solutions saturated with CO_2 at various HFr concentrations and solution pH values. The potentiodynamic sweeps are shown in Fig. 10 and the corresponding corrosion rates are plotted in Fig. 11. Fig. 10(a) compares the potentiodynamic polarization sweeps of X65 electrode at 30 °C, pH 4, and 2000 rpm, without and with 1.41 mM of undissociated HFr , in N_2 - and CO_2 -sparged solutions respectively. According to this figure, aqueous CO_2 , or more precisely its hydrated form – the weak carbonic acid H_2CO_3 , behaves similarly to the weak HFr acid, in the way it contributes to the cathodic reaction by buffering. H_2CO_3 dissociation replenishes the consumed H^+ ions [30], resulting in an increase in the limiting current density, just as HFr does.

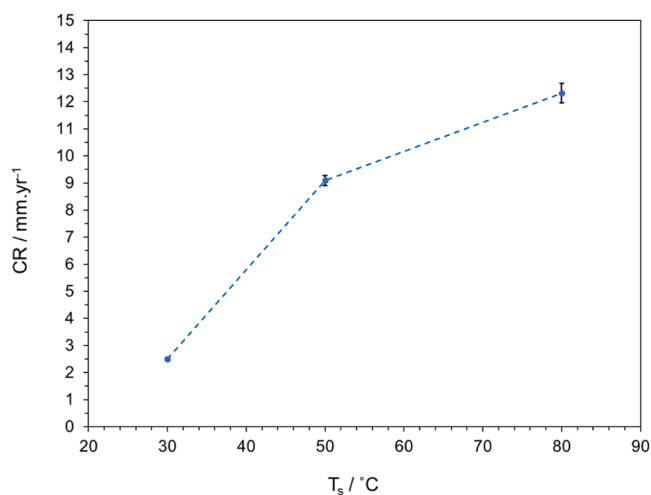


Fig. 7. Corrosion rates of X65 steel in N_2 -sparged 1 wt.% $NaCl$ solution at 1.41 mM undissociated HFr , 2000 rpm RDE, pH 4, and at various temperatures (error bars show minimum and maximum values of corrosion rate at each temperature).

When the system contains HFr and H_2CO_3 , both species contribute to the “buffering effect” to supply extra H^+ ions and increase the limiting current density. Since, under these conditions, the corrosion rate is predominantly under charge transfer control, the increase in limiting current density only slightly increases the corrosion rates, as shown in Fig. 11(a).

In Fig. 10(b), the polarization behavior of X65 electrode in a CO_2 -sparged environment at 30 °C and 1.41 mM of undissociated HFr is shown at two different bulk solution pH. Generally, the behavior is the same as was shown above for a pure HFr aqueous solution sparged with N_2 . The comparison between corrosion rates corresponding to solutions with only HFr and solutions with both HFr and H_2CO_3 , at pH 4 and 5 are shown in Fig. 11(b). The slight overall decrease in the corrosion rate with increase in pH can be attributed to the enhanced anodic reaction rate offsetting the retardation in the cathodic reaction rates, as discussed above. Overall, the corrosion rates in a system containing both HFr and H_2CO_3 are higher than in a system that only contains HFr . This trend is observed at both pH 4 and pH 5, as shown in Fig. 11(b).

3.3. Comparison of polarization behavior of mild steel in formic and acetic acid environments

Fig. 12(a) shows the effect of HAc concentration in a N_2 -sparged environment at pH 4, 2000 rpm, and 30 °C. To provide the comparison with HFr , the polarization sweeps in a solution with 1.41 mM of undissociated HFr at the same experimental conditions is also plotted in Fig. 12(b).

The results in Fig. 12 and those previously shown in Fig. 2 show that the increase in the concentration of undissociated organic acids (both HFr and HAc) significantly influences the limiting current region, however it has no significant effect on the charge transfer region of hydrogen evolution. It is noted that distinguishing the charge transfer region at low concentrations of HAc is challenging and the mentioned observation is mainly based on comparing the sweep at 1.41 and 14.1 mM HAc (blue and yellow curves).

The effect of HAc on the anodic reaction is different. According to Fig. 12(a), an increase in the concentration of undissociated HAc leads to a decrease in the anodic current density and subsequently a decrease in the corrosion rate [31]. It is noted that the anodic inhibition by HAc occurs at relatively high concentrations and at low concentration the two acids have similar influence on the anodic reaction. Kahyarian et al. [14] attributed this rather weak inhibition effect of HAc to its adsorption on the metal surface that blocks the active sites of electron transfer reactions. Such decrease in anodic current density is not observed with the increase in concentration of HFr (Fig. 2), which implies that in the presence of HFr , a similar adsorption phenomenon does not occur to the extent as is observed in the presence of HAc . This difference leads to a higher corrosivity of the solution in the presence of HFr compared to HAc at 30 °C.

Additionally, in Fig. 12(b) it appears that the current density in the charge transfer region for the cathodic reaction is higher for HFr than that for HAc at the same potentials. It was established by Kahyarian et al. [29] that the presence of HAc does not retard the charge transfer rate for the cathodic reaction – reduction of H^+ ions, also seen in Fig. 12(a). Then the present results suggest that the HFr must lead to an acceleration of the same reaction, however this was not clearly observable under the conditions covered in this study (see from Fig. 2). In order to understand and explain this behavior, a more extensive set of experiments needs to be conducted, preferably at even lower temperatures (e.g., 10 °C) when the charge transfer section of the cathodic polarization curve is more distinct.

Fig. 13(a) compares the measured limiting current densities of an X65 electrode in solutions with different concentrations of undissociated HAc and HFr under nominally identical experimental conditions (N_2 -saturated 1 wt.% $NaCl$ solution at 30 °C, 2000 rpm RDE, pH 4). According to this figure, the cathodic limiting current densities in the

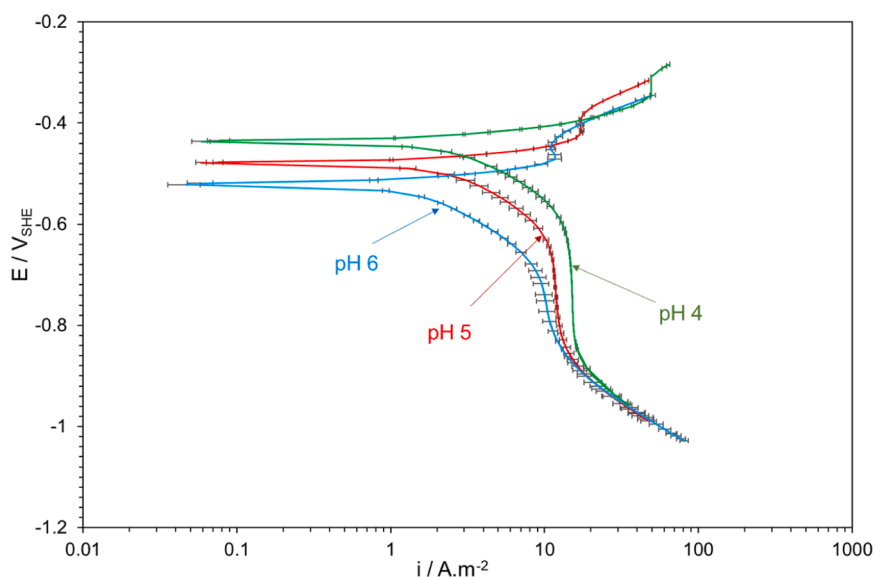


Fig. 8. Polarization behavior of X65 steel in N_2 -sparged 1 wt.% NaCl solution at 1.41 mM undissociated *HFr*, 30 °C, 2000 rpm RDE, and various solution pH (error bars show minimum and maximum values of current density at each potential).

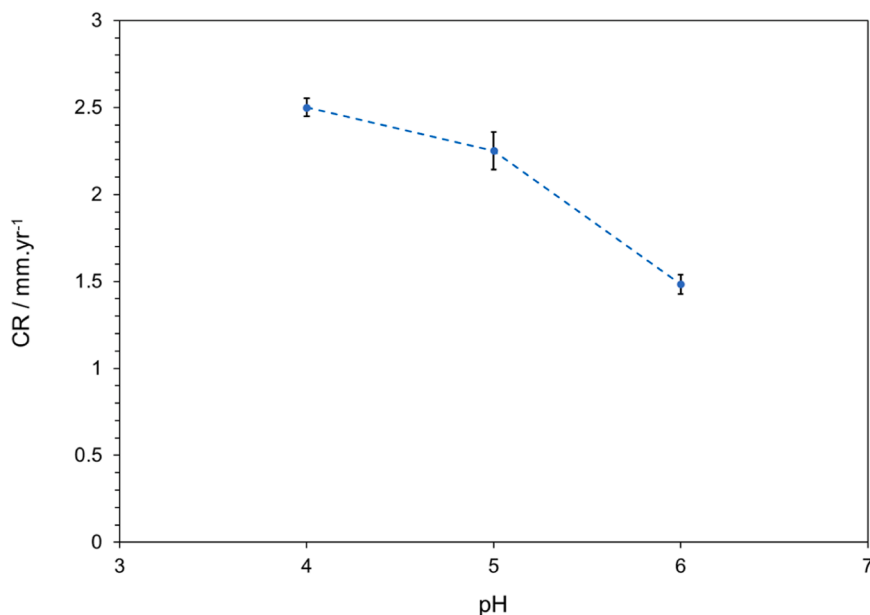


Fig. 9. Corrosion rates of X65 steel in N_2 -sparged 1 wt.% NaCl solution at 1.41 mM undissociated *HFr*, 30 °C, 2000 rpm RDE, and various solution pH (error bars show minimum and maximum values of corrosion rate at each pH).

presence of the two organic acids are quite similar, which is a surprise. Even if the molar concentrations of each “undissociated” organic acid is the same in these comparisons, the difference in their molecular weight implies a slightly higher diffusivity for *HFr* ($1.46 \times 10^{-9} \text{ m}^2/\text{s}$ for *HFr* and $1.29 \times 10^{-9} \text{ m}^2/\text{s}$ for *HAc*) [32,33]. Furthermore, as compared to *HAc*, *HFr* is a stronger acid that dissociates more readily, what should result in a stronger buffering effect. Yet, this seems to play a negligible role when it comes to the magnitude of the resulting limiting current density. Further investigation into this observation is required.

The plot in Fig. 13(b) shows the corrosion rate with different concentrations of *HFr* and *HAc* at 30 °C. In the case of *HAc*, the corrosion rate decreases with the concentration as a result of previously mentioned anodic inhibition [14–17], which results in lower corrosion rates compared to those at similar concentrations of *HFr*. The corrosion rate with *HFr* in the solution increases by addition of 0.141 M

undissociated *HFr* and it shows a slight increase with the further increase in the concentration, as discussed earlier. In the case of *HFr*, not only anodic inhibition is absent, but also a slight acceleration of cathodic reaction in the charge transfer region (observed at 1.41 mM concentration) leads to higher corrosion rates compared to *HAc* at similar concentrations.

Additional experiments conducted at different temperatures, with 1.41 mM of undissociated organic acids showed that the behavior of *HFr* and *HAc* deviates at higher temperatures ($30 \text{ °C} \leq T \leq 80 \text{ °C}$). The comparison of related polarization curves is presented in Fig. 14(a). The variation of cathodic limiting current density versus temperature in the presence of 1.41 mM undissociated organic acids at pH 4 is depicted in Fig. 14(b). While the limiting current density in the presence of the two acids are similar at 30 °C, as the temperature increases, the limiting current density for the same concentration of undissociated *HFr* is

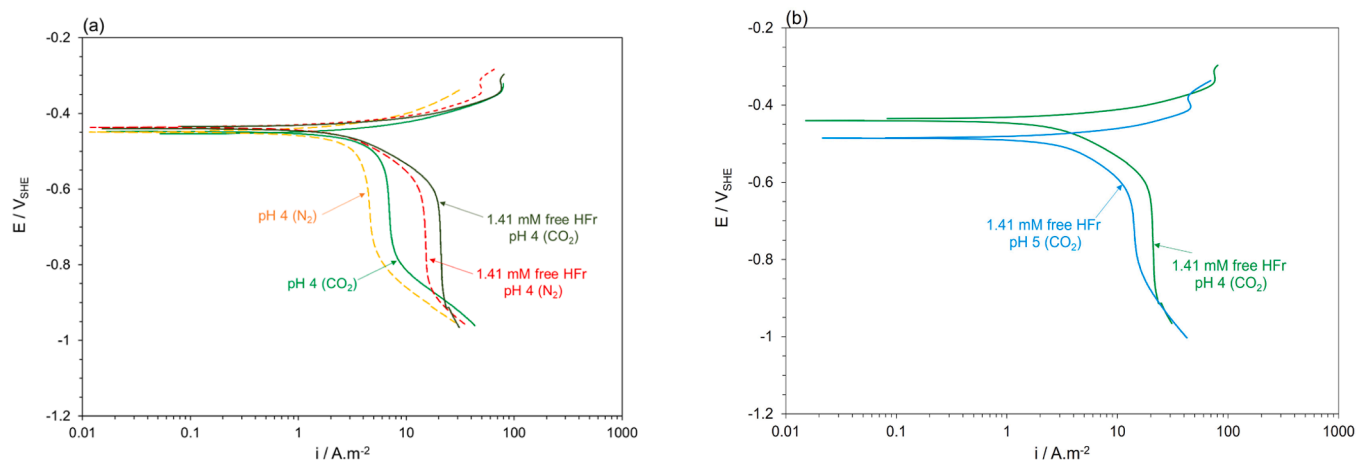


Fig. 10. Polarization behavior of X65 steel in 1 wt.% NaCl solution at 30 °C, 2000 rpm RDE in (a) N_2 - and CO_2 -sparged solutions, pH 4, 0 and 1.41 mM undissociated HFr and (b) CO_2 -sparged solutions, 1.41 mM undissociated HFr at solution pH 4 and 5.

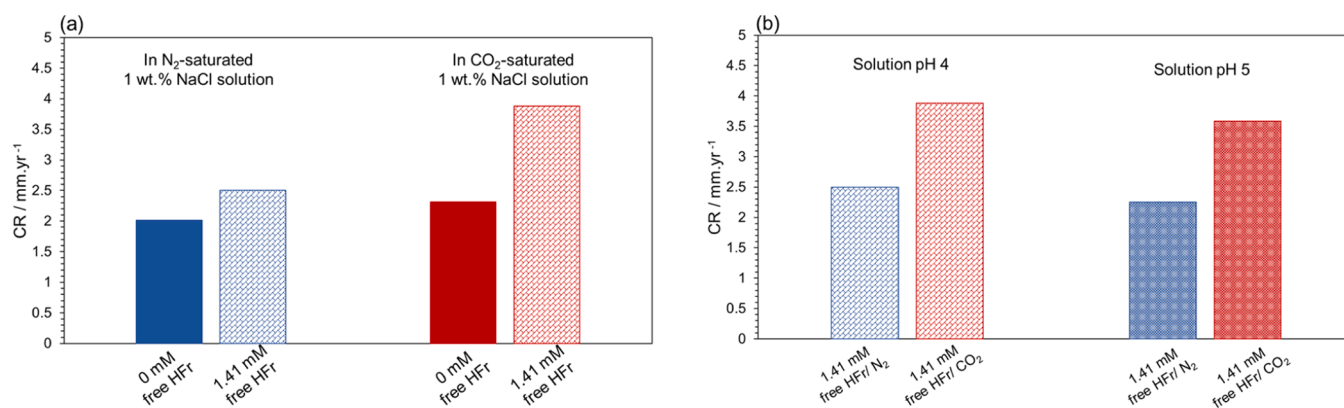


Fig. 11. Corrosion rates of X65 steel in 1 wt.% NaCl solution at 30 °C, 2000 rpm RDE in (a) N_2 and CO_2 -sparged solutions, pH 4, 0 and 1.41 mM undissociated (free) HFr concentrations and (b) N_2 and CO_2 -sparged solutions, 1.41 mM undissociated (free) HFr at solution pH 4 and 5.

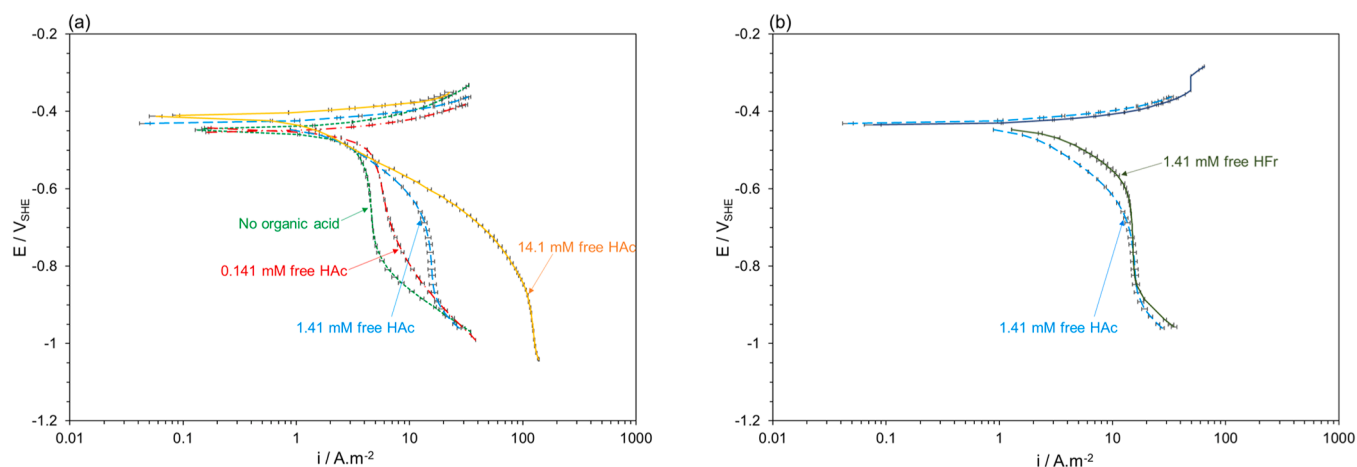


Fig. 12. (a) Polarization behavior of X65 steel in N_2 -sparged 1 wt.% NaCl solution at 30 °C, pH 4, 2000 rpm RDE, and various undissociated HAc concentrations and (b) comparison between 1.41 mM HFr and 1.41 mM HAc (error bars show minimum and maximum values of current density at each potential).

significantly lower than that for HAc .

One reason for this difference in behavior could be because of the diffusivities of HFr and HAc . The higher limiting current density observed for HAc at 80 °C may suggest a higher diffusivity of HAc than HFr . However, this explanation seems contrary to intuition considering

the molecular weights of HFr and HAc . A possible supposition is that there could be a difference in temperature dependence of diffusivity between HFr and HAc .

An alternative rationale could be related to the temperature dependence of the kinetics of dissociation for HFr and HAc . The value of pK_a

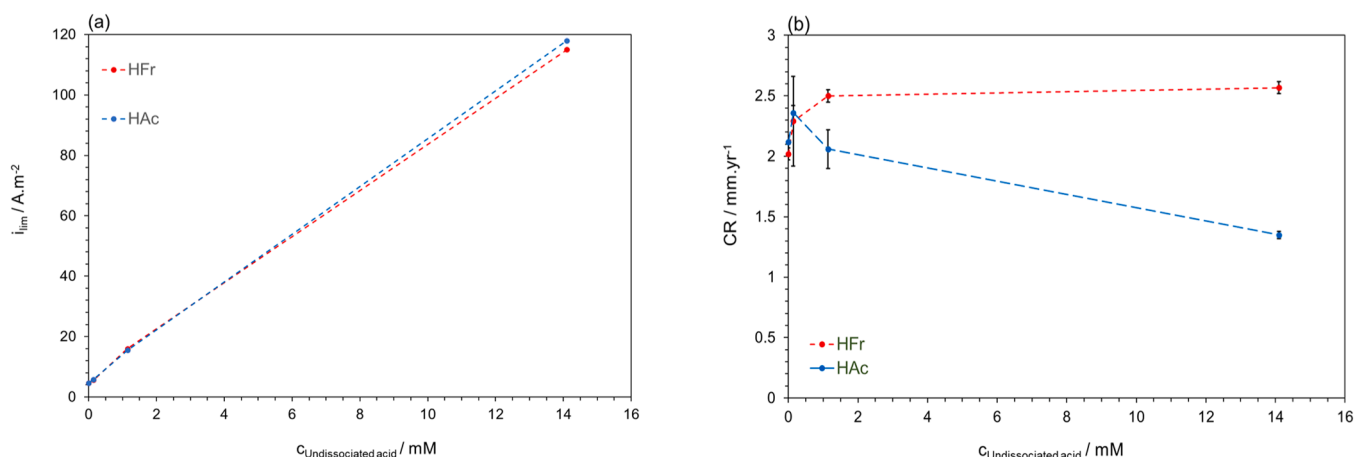


Fig. 13. (a) Cathodic limiting currents and (b) Corrosion rates of X65 steel in N_2 -sparged 1 wt.% $NaCl$ solution at 30 °C, 2000 rpm RDE, pH 4, at 0, 0.14, 1.41, & 14.1 mM undissociated *HFr* and *HAc* concentrations.

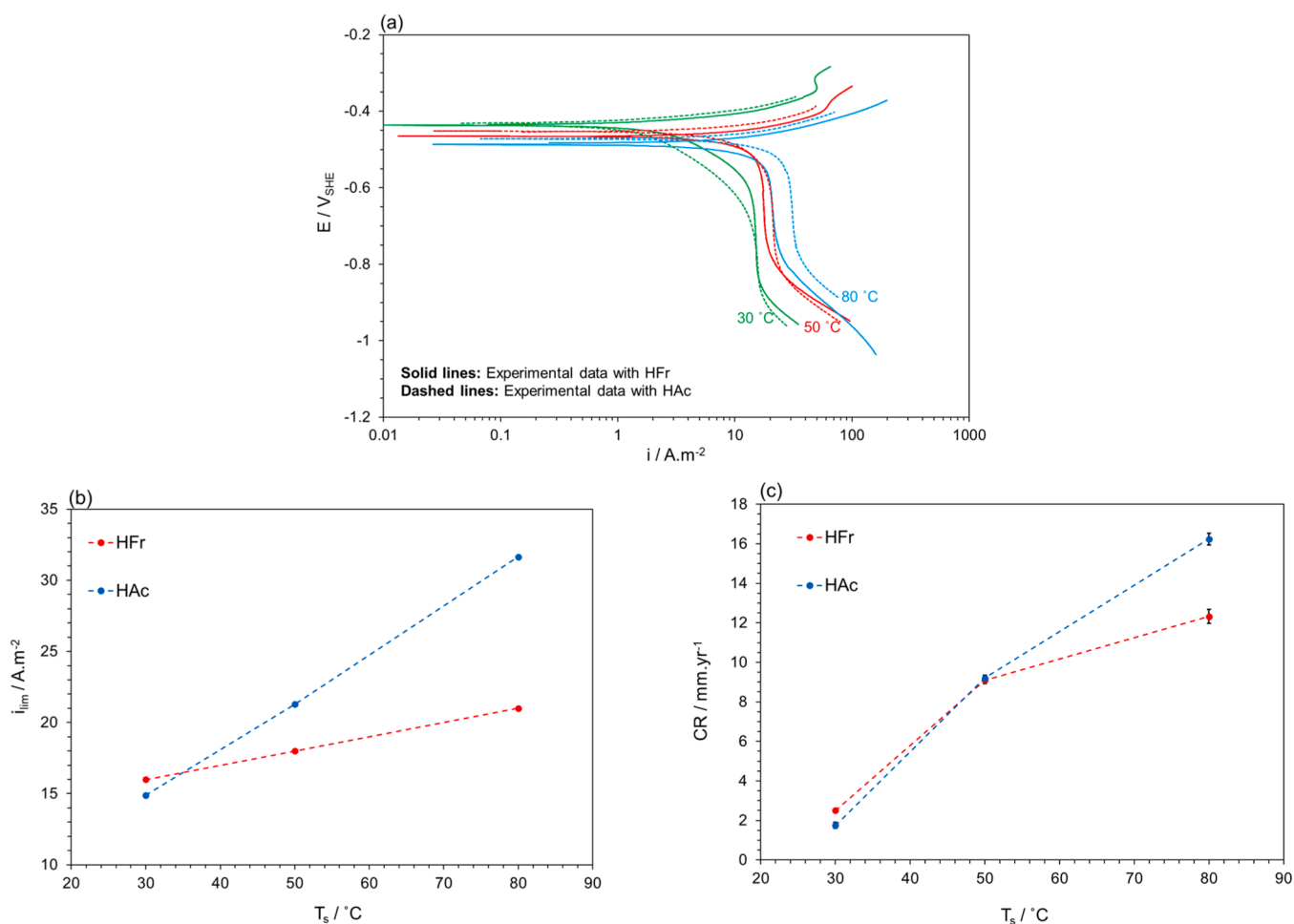


Fig. 14. (a) Polarization behavior of X65 steel in N_2 -sparged 1 wt% $NaCl$ solution at 1.41 mM undissociated *HFr* or *HAc*, 2000 rpm RDE, pH 4, at various temperatures, (b) Cathodic limiting currents and (c) Corrosion rates of X65 steel in N_2 -sparged 1 wt.% $NaCl$ solution with 1.41 mM undissociated *HFr* or *HAc* at 2000 rpm RDE, pH 4, 30°C, 50°C and 80°C.

gives quantitative information regarding the acid strength, i.e., the higher the pK_a , the weaker the acid. By comparing the pK_a ($pK_a = -\log K_a$) values of *HAc* (4.76 at 30 °C and 4.86 at 80 °C) and *HFr* (3.75 at 30 °C and 3.86 at 80 °C) [18,34], it is clear that *HFr* is a stronger acid than *HAc* and dissociates more readily in the solution under the same experimental conditions. This comparison of dissociation constants for

acetic and formic acids is shown in Fig. 15. The extent of buffering effect induced by the presence of *HFr* and *HAc* is similar as the concentration of undissociated organic acids are maintained constant under the different experimental conditions. However, it seems as if the limiting current densities associated with the dissociation of *HAc* are slightly greater. This becomes more apparent at higher temperatures. At both 50°C and

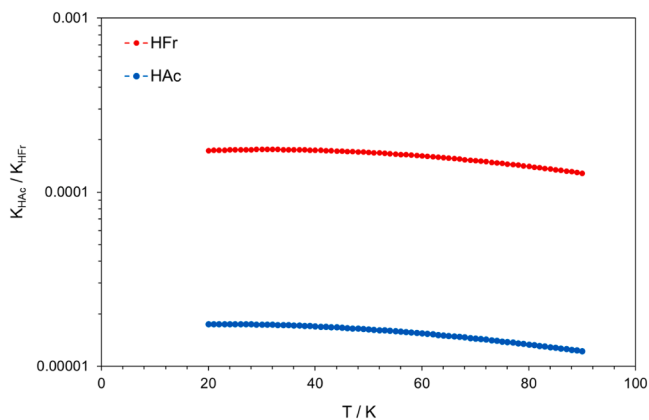


Fig. 15. Equilibrium constant value for *HFr* and *HAc* dissociation reaction versus temperature (The $K(T)$ functions for *HFr* and *HAc* are reported [18] and [19], respectively).

80°C, when the kinetics of reactions are increased due to the increase in temperature and the cathodic reaction is predominantly under limiting current-control, *HAc* dissociates less readily as compared to *HFr*, and contrary to what would be expected, *HAc* limiting current density is higher.

Another possible and more plausible reason to keep in mind is the potential inaccuracy of expressions available in the literature regarding the dependency of equilibrium constant for both *HFr* and *HAc*. While three temperature functions were found in the literature for K_{HAc} [19,34,35], there was only source for such function for K_{HFr} [18]. The three functions for K_{HAc} were compared and all provided reasonably similar values and one [19] was selected for both experimentation and modeling. One might speculate that the temperature function for K_{HFr} is not accurate at least at higher temperatures. Such inaccuracy will result in errors in speciation calculations and hence possible faulty results. Providing a more accurate function for K_{HFr} requires further investigations. However, its possible influence on the results of the current study will be discussed in more detail in the modeling section.

The corrosion rates of steel increase with temperature in the presence of both *HFr* and *HAc*. This increase is partly attributed to a greater influence of the limiting current density value on the corrosion rate at higher temperatures. This is because the reaction is predominantly under limiting current-control mechanism at higher temperatures. Moreover, the difference in limiting current densities observed between *HFr* and *HAc* at different temperatures is clearly reflected in the corrosion rates, as shown in Fig. 14(c).

3.4. Modeling

In order to model the polarization behavior of mild steel exposed to an environment containing weak acids such as H_2CO_3 , H_2S , and organic acids, a mechanistic model needs to account for the anodic and cathodic charge transfer reactions and the limiting current rates. The latter step, which in this case amounts to calculating the cathodic limiting current density due to buffering can be rather involved as we cannot use the standard expressions for a mass transfer limiting current density. The weak acids present in the system act as an extra source of H^+ ions and contribute to the hydrogen reduction reaction through the “buffering effect”. An example of one such mechanistic model can be found in a work by Kahyarian et al. [14], in which a comprehensive model is formulated amounting to a set of partial differential equations that need to be resolved using numerical methods. A more recent model developed by Nescic and Madani Sani [25,36] presents a simpler approach and provides an explicit equation to calculate the limiting current density in the presence of H_2CO_3 . A similar approach will be deployed here for the case of *HFr*.

The anodic dissolution rate for iron, which is under charge transfer control is calculated as [37]:

$$i_{\alpha,Fe} = i_{0,Fe} \cdot 10^{-\frac{\eta}{b_a}} \quad (5)$$

Where $i_{0,Fe}$ is the exchange current density of dissolution of iron in A/m^2 , η is the overpotential (with respect to $E_{rev(Fe^{2+})} = -0.488 V_{SHE}$), b_a is the anodic Tafel slope (V/decade):

$$b_a = \frac{2.303RT}{\alpha_a F} \quad (6)$$

In Eq. (6), F is the Faraday constant and α_a is set to 1.5 according to Bockris et al. [28]. The dependence of the exchange current density for iron ($i_{0,Fe}$) on temperature is given by Arrhenius-type equation:

$$i_{0,Fe} = i_{0,Fe}^{ref} \left(\frac{c_{OH^-}}{c_{OH^-}^{ref}} \right)^{a_1} \cdot e^{-\frac{\Delta H}{R} \left(\frac{1}{T} - \frac{1}{T_{ref}} \right)} \quad (7)$$

In Eq. (7), $i_{0,Fe}^{ref}$ ($0.1 A \cdot m^{-2}$) is the reference exchange current density at reference temperature T_{ref} (293.15 K), and reference potential $E_{ref(Fe^{2+})}$ ($-0.488 V$ vs V_{SHE}) [38]. The ΔH ($65 kJ/mol$) is the enthalpy of activation for the iron dissolution reaction. ΔH was found through fitting the experimental data to the developed model and was higher than the previously reported value ($40 kJ/mol$) by other researchers [37]. The reason for this discrepancy is related to the selection of the reference $E_{ref(Fe^{2+})}$ which influences the magnitude of ΔH , given that not only $i_{0,Fe}$ but also the Tafel slope b_a depend on temperature. The reference concentration $c_{OH^-}^{ref}$ ($10^{-10} M$) [36] is used to account for the effect of pH on the rate of anodic iron dissolution and a_1 is the reaction order with respect to OH^- concentration and is found to be equal to 0.5 by fitting the developed model to the experimental data.

The charge transfer controlled cathodic current density is calculated as follows [37]:

$$i_{\alpha,H^+} = i_{0,H^+} \cdot 10^{-\frac{\eta}{b_c}} \quad (8)$$

where i_{0,H^+} is the exchange current density, η is the over potential (with respect to $E_{rev(H^+)} = -0.24 V_{SHE}$), and b_c is the cathodic Tafel slope (V/decade):

$$b_c = \frac{2.303RT}{\alpha_c F} \quad (9)$$

In this equation, α_c is set to 0.48, which agrees well with current experimental data, a similar value of 0.5 for α_c has been used by other researchers [28], and F is the Faraday constant. The dependence of the exchange current density on the temperature is modeled with an Arrhenius-type equation [36]:

$$i_{0,H^+} = i_{0,H^+}^{ref} \left(\frac{c_{H^+}}{c_{H^+}^{ref}} \right)^{a_1} \cdot e^{-\frac{\Delta H}{R} \left(\frac{1}{T} - \frac{1}{T_{ref}} \right)} \quad (10)$$

In Eq. (10), i_{0,H^+}^{ref} ($0.05 A \cdot m^{-2}$), T_{ref} (293.15 K), and $c_{H^+}^{ref}$ ($10^{-4} M$) [36], are the reference exchange current density, temperature, and H^+ reference concentration, respectively. ΔH ($30 kJ/mol$) is the enthalpy of activation for H^+ reduction reaction. The value of ΔH was found through fitting the experimental data to the developed model and was equal to the value found by Nescic et al. [37] through an experimental approach. a_1 is the constant reaction order with respect to H^+ concentration and is equal to 0.5 [38].

With *HFr* present in solution, as H^+ is consumed by the cathodic reaction, the free *HFr* in the boundary layer will dissociate to provide more H^+ ions as shown by Reaction (2). With the depletion of both H^+ and free *HFr* in the boundary layer, diffusion of both species will occur because of their concentration gradients across the boundary layer. The limiting current is reached when the diffusion of both species to the

metal surface cannot keep up with the reduction of H^+ at the metal surface.



In order to calculate the total limiting current density with only one cathodic reaction (H^+ reduction), co-diffusion of both H^+ and free HFr and the buffering effect by the chemical dissociation reaction (2) in the mass transfer boundary layer should be accounted for. Following Dognadze [39], Sani [36] presented a mechanistic model and derived an equation for the limiting current in the presence of HAc , which is here adapted for HFr :

$$i_{lim} = 1000F(D_{H^+}) \left(\frac{\lambda K_{HFr} (D_{HFr} c_{HFr, b}^{eq} + D_{H^+} c_{H^+, b}^{eq})}{(D_{HFr} c_{Fr, b}^{eq} + D_{H^+} \lambda K_{HFr}) \delta_m} \right) \quad (13)$$

In this manuscript D_i (m^2/s) and c_i (M) refer to the diffusivity and the concentration of species i , respectively and $c_{i,b}^{eq}$ refers to the bulk equilibrium concentration of species i . In our case i can be H^+ or HFr . In Eq. (13), K_{HFr} is the equilibrium constant for the HFr dissociation reaction (presented earlier in Eqs. (3) and (4)) is equal to:

$$K_{HFr} = \frac{k_{f,HFr}}{k_{b,HFr}} = \frac{c_{Fr, b}^{eq} c_{H^+, b}^{eq}}{c_{HFr, b}^{eq}} \quad (14)$$

In Eq. (13), λ is a kinetic parameter defined as:

$$\lambda = \frac{\delta_m}{\delta_r} \coth \left(\frac{\delta_m}{\delta_r} \right) \quad (15)$$

In this equation and in Eq. (13), δ_m (m) is a weight averaged mass transfer boundary layer thickness defined as:

$$\delta_m = \frac{c_{HFr, b}^{eq} \delta_{m, HFr} + c_{H^+, b}^{eq} \delta_{m, H^+}}{c_{HFr, b}^{eq} + c_{H^+, b}^{eq}} \quad (16)$$

Here $\delta_{m, HFr}$ (m) and δ_{m, H^+} (m) can be calculated using:

$$\delta_{m, i} = \frac{D_i}{k_{m, i}} \quad (17)$$

$$k_{m, i} = 0.62 D_i^{2/3} \omega^{1/2} \nu^{-1/6} \quad (18)$$

In these equations, $k_{m, i}$ ($m s^{-1}$) is the mass transfer coefficient for species i , ω ($rad s^{-1}$) is angular velocity of the RDE and ν (m^2/s) is the kinematic viscosity of the aqueous solution.

In Eq. (15) a new parameter is used, the “chemical reaction boundary layer thickness (δ_r) (m)”, which is defined as:

$$\delta_r = \frac{1}{\sqrt{\frac{k_{f,HFr}}{D_{HFr}} + \frac{k_{b,HFr} c_{Fr^-}}{D_{H^+}}}} \quad (19)$$

Here, it should be mentioned that the effect of salt ($NaCl$) concentration on the physical properties of the aqueous solution were considered while constructing the model [36,38,40]. Density of water and the brine (1 wt. $NaCl$ solution) in g/cm^3 are calculated as follows [41]:

$$\begin{aligned} \rho_w &= 1 + 10^{-6} \times (-80T - 3.3T^2 + 0.00175 T^3 + 489 \left(\frac{P}{10}\right) - (2TP) \\ &+ \left(0.016T^2 \times \left(\frac{P}{10}\right)\right) - \left(1.3 \times 10^{-5} \times T^3 \times \left(\frac{P}{10}\right)\right) \\ &- \left(0.333 \left(\frac{P}{10}\right)^2\right) - \left(0.002T \times \left(\frac{P}{10}\right)^2\right) \end{aligned} \quad (20)$$

$$\begin{aligned} \rho_{brine} &= \rho_w + \left(\frac{wt_{NaCl}}{100}\right) \times \left(0.668 + 0.44 \times \left(\frac{wt_{NaCl}}{100}\right) + 10^{-6} \right. \\ &\times \left(300 \left(\frac{P}{10}\right) - 2400 \left(\frac{P}{10}\right) \times \left(\frac{wt_{NaCl}}{100}\right) + T \right. \\ &\times \left. \left. \left(80 + 3T - 3300 \times \left(\frac{wt_{NaCl}}{100}\right) - 13 \left(\frac{P}{10}\right) + 47 \left(\frac{P}{10}\right) \times \left(\frac{wt_{NaCl}}{100}\right)\right)\right)\right) \end{aligned} \quad (21)$$

In Eqs. (20) and (21), T is the temperature in $^\circ C$, P is the total pressure in bar, wt_{NaCl} is the weight percentage of $NaCl$ in the solution (brine).

As for the water and brine dynamic viscosities (in $kg/m\cdot s$) the following equations were used, one of which is an alternative equation for water density (in g/cm^3) [42]:

$$\begin{aligned} \rho_w^* &= 10^{-3} (134.136579 - 4077.438 \times 10^{(-0.00556126409T)} + 16319.2756 \\ &\times 10^{(-0.01071492347T)} + 1370.91355 \times 10^{(-0.000546294495T)} \\ &+ 0.445861703 \left(\frac{P}{10}\right)^2 - 0.000451029739 * \left(\frac{P}{10}\right)^2) \end{aligned} \quad (22)$$

$$\begin{aligned} \mu_w &= \exp(2885317T^{-2} - 11072.577T^{-1} - 9.0834095 + 0.030925651T \\ &- 0.0000274071T^2 + \rho_w^* \times (-1928385.1T^{-2} + 5621.6046T^{-1} \\ &+ 13.82725 - 0.047609523T + 0.000035545041T^2)) \end{aligned} \quad (23)$$

$$\begin{aligned} \mu_{brine} &= \mu_w \times \exp(0.1168643 m_{NaCl} - 0.001215 m_{NaCl}^2 \\ &+ 0.0001553 m_{NaCl}^3) \end{aligned} \quad (24)$$

In Eqs. (22)–(24) T is the temperature in K, P is the total pressure in bar, and m_{NaCl} is $NaCl$ molality ($mol kg^{-1}$), calculated from its weight percentage in the solution as follows:

$$m_{NaCl} = \frac{10wt_{NaCl}}{55.4428 \left(1 - \frac{wt_{NaCl}}{100}\right)} \quad (25)$$

For diffusion coefficients, temperature and salt concentration corrections were both considered. For H^+ , the temperature correction was based on Appelo model [43]:

$$D_{H^+}^T = D_{ref} \times \left(\frac{\mu_{brine}(298.15(K))}{\mu_{brine}(T(K))}\right) \times \left(\frac{T}{298.15}\right) \times \exp\left(\frac{763}{T} - \frac{763}{298.15}\right) \quad (26)$$

In Eq. (26), D_{ref} H^+ is $9.31 \times 10^{-9} m^2/s$ (its diffusion coefficient at 298.15 K), $\mu_{brine}(298.15 K)$ is the viscosity of brine (solution) at or 298.15 K, and T is the temperature in K.

The concentration correction for $D_{H^+}^T$ is applied as follows to calculate D_{H^+} (m^2/s) that is used in the model [44]:

$$D_{H^+} = D_{H^+}^T \times \left(1 - \frac{0.512 \times M_{NaCl}^{0.5}}{2}\right) \quad (27)$$

In Eq. (27), M_{NaCl} is the molarity of $NaCl$ and calculated as follows:

$$M_{NaCl} = \frac{0.001 m_{NaCl} \times \mu_{brine}}{\left(1 + \frac{wt_{NaCl}}{100 - wt_{NaCl}}\right)} \quad (28)$$

The dependency of the diffusivity (D) of species involved in reactions on temperature is generally described by the Stokes-Einstein equation [37], which was used for D_{HFr} :

$$D^T = D_{ref} \times \frac{T}{T_{ref}} \times \frac{\mu_{brine, ref}}{\mu_{brine}} \quad (29)$$

In Eq. (29) D is the diffusivity in m^2/s , T is the temperature in K and μ is the dynamic viscosity of the solution (brine, as calculated in Eq. (24))

in kg/m·s. D_{ref} at 298.15 K for HFr is 1.46×10^{-9} m²/s. μ_{ref} is the viscosity of the solution at $T_{ref} = 298.15$ K.

The concentration correction for D_{HFr}^T is applied as following to calculate D_{HFr} (m²/s) that is used in the model [44]:

$$D_{HFr} = D_{HFr}^T \times \left(1 - \frac{0.512 \times M_{NaCl}^{0.5}}{2}\right) \quad (30)$$

In this study to simplify the model, we did not consider the water reduction reaction that occurs at more negative potentials. The total cathodic current density, assuming a first-order reaction is then equal to:

$$i_{c,H^+} = \frac{1}{\frac{1}{i_{a,H^+}} + \frac{1}{i_{lim}}} \quad (31)$$

The net current density is the sum of anodic and cathodic currents, where the cathodic current is negative by convention. To plot the polarization behavior over the desired range of potential, the total current density is calculated as follows:

$$i = |i_{a,Fe} - i_{c,H^+}| \quad (32)$$

The corrosion current was found by solving the charge transfer balance at the metal surface (anodic reaction rate equal cathodic reaction rate):

$$i_{a,Fe} = i_{c,H^+} \quad (33)$$

for the unknown corrosion potential and then replacing this potential into either of these partial currents.

3.5. Comparison between the experimental data and model

In Fig. 16, the polarization curves obtained from X65 steel RDE in a N_2 -sparged 1 wt.% NaCl solution at 30 °C, pH 4 and different concentrations of undissociated HFr are compared with the modeled data. The anodic behavior and the charge transfer-controlled region of the cathodic curve is captured by the model and the modeled values are close to the experimental data (without considering the transition and pre-passivation regions of the anodic curve [45]). In the absence of HFr the model shows a slight underprediction which is acceptable.

In the limiting current section of the cathodic curve, an over prediction is observed in the presence of HFr . One possible explanation for

this discrepancy between the experimental and modeled data could be related to the inaccurate values of the constants describing the physical properties of the system used in the model; another could be related to the fact that in the assumption used in developing the model, the HFr dissociation reaction (Reaction (2)) is in equilibrium in the boundary layer, what might not be true in reality. Therefore the values of $c_{HFr,b}^{eq}$, $c_{H^+,b}^{eq}$, and $c_{Fr,b}^{eq}$ used in Eq. (13) could be inaccurate.

Fig. 17(a) presents the comparison between the modeled and the experimental data at pH 4 and a constant concentration of undissociated HFr (1.41 mM) at 50 °C and 80 °C. According to this figure, while the prediction is quite accurate at the charge transfer-controlled region of the cathodic reaction, the modeled and experimental limiting current densities are 67 and 106 % different at 50 °C and 80 °C, respectively. In this study, much care was taken to assure the accuracy of the experimental results through the addition of accurate concentrations of HFr , control of pH, and temperature. The difference in the experimental and modeled limiting currents at 50 °C and 80 °C could be related to the possible deviation of HFr dissociation reaction from equilibrium at these two temperatures that is not considered in the model or the inaccuracy of the temperature dependence of K_{HFr} value. While the effect of deviation of other determining factors such as diffusion coefficient (D_{HFr}) and the forward and backward rates of HFr dissociation reaction (Reaction (2)) from the literature values were also considered and investigated, modifying none of them could result in accurate predictions for the relatively wide range of experimental conditions in this study. However, as shown in Fig. 17(b), by multiplying the K_{HFr} value at 80 °C by correction factor of 2, the model prediction becomes closer to the actual experimental value. Using this correction factor at other experimental conditions improves the model accuracy as well. However, due to the uncertainty and limited amount of data at high temperatures, the use of this factor was limited to the data acquired at 80 °C. The uncertainty regarding the dependence of K_{HFr} on temperature requires further investigations which is out of scope of the current study.

Covering the other experimental conditions, as shown in Fig. 18, at 30 °C, pH 5 and pH 6 the model captures the anodic and cathodic polarization behavior at the charge transfer-controlled region. The prediction of the limiting current densities at these conditions is rather accurate.

The performance of the model is further examined by comparing the

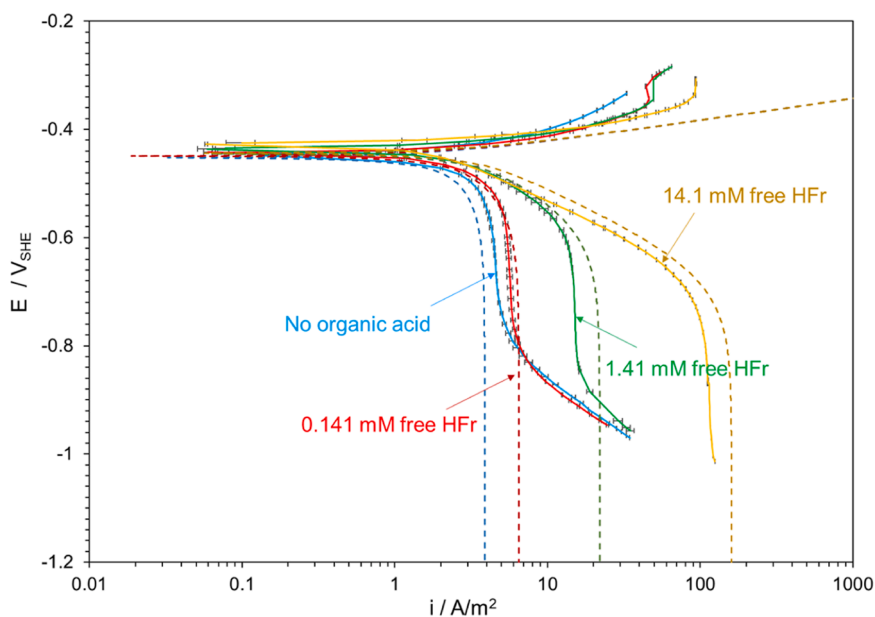


Fig. 16. Comparison of the experimental polarization behavior of X65 steel with the model in N_2 -sparged 1 wt.% NaCl solution at 30 °C, 2000 rpm RDE, pH 4 and HFr concentrations of 0 mM, 0.141 mM, 1.41 mM, and 14.1 mM (error bars show minimum and maximum values of current density at each potential).

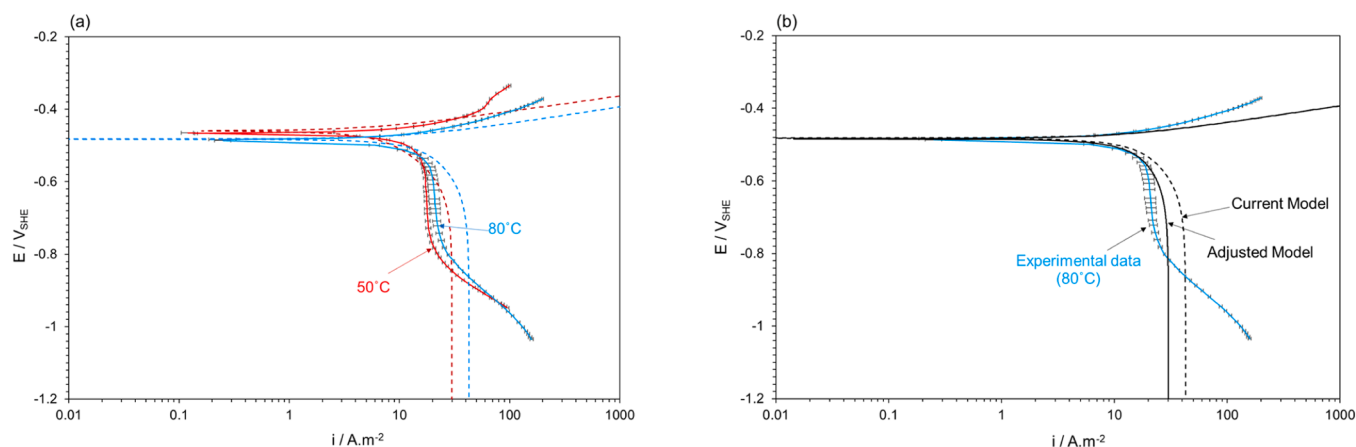


Fig. 17. (a) Comparison of the experimental polarization behavior of X65 steel with the model in N_2 -sparged 1 wt.% NaCl solution at 1.41 mM undissociated HFr , 2000 rpm RDE, pH 4, 50°C and 80°C and (b) comparison of current model and adjusted model at 80°C (error bars show minimum and maximum values of current density at each potential).

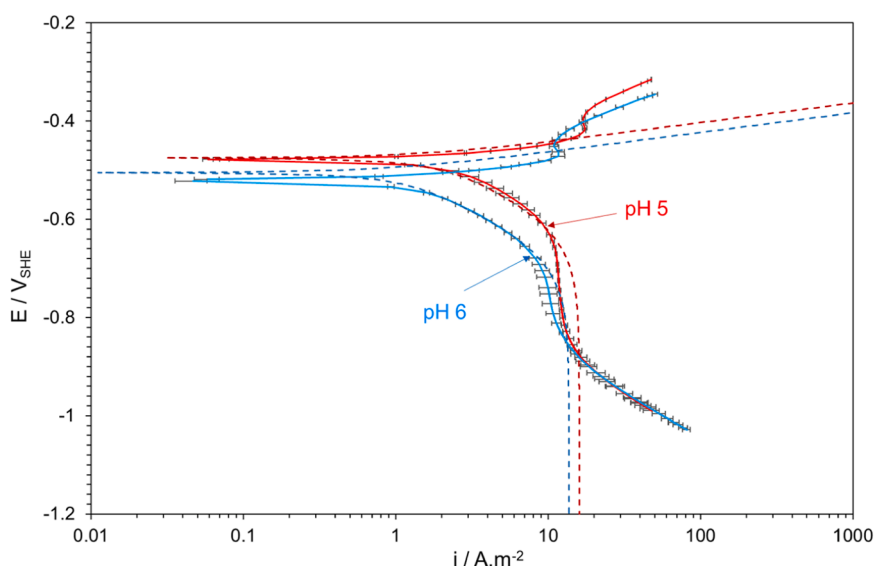


Fig. 18. Comparison of the experimental polarization behavior of X65 steel with the model in N_2 -sparged 1 wt.% NaCl solution at 1.41 mM undissociated HFr , 30 °C, 2000 rpm RDE, pH 5 and pH 6 (error bars show minimum and maximum values of current density at each potential).

estimated corrosion rate with the experimental data obtained by linear polarization resistance (LPR) measurements. Fig. 19 shows this comparison. As expected, the model is reasonably accurate at 30 °C at different pH, and different concentrations of undissociated HFr , however it shows a discrepancy with the experimental corrosion rate data at the highest concentration of HFr and at higher temperatures. This could be the result of a possible inaccuracy in the current equation for K_{HFr} and requires modification to capture the real behavior of HFr as mentioned in the discussion earlier.

4. Conclusions

The following conclusions can be drawn from this study:

- HFr contributes to the corrosion of steel through its chemical dissociation, which induces the buffering effect by replenishing H^+ ions. This contributes to an increase in limiting current density with increase in concentration of HFr .
- HFr does not significantly influence the anodic dissolution of mild steel at the studied range of potential.

- In the presence of two weak acids (HFr and H_2CO_3) an additive increase in the limiting current density of the cathodic reaction was observed which is attributed to the additive buffering effect.
- While HAc slightly retards the anodic reaction, resulting in a decrease in the corrosion rate with increasing its concentration at 30 °C, the same effect was not observed for HFr .
- Although HFr is more corrosive than HAc at 30 °C, it was observed that HAc is more corrosive than HFr at the higher temperatures tested in this study (50 °C and 80 °C) and results in greater limiting current densities.
- The difference between the polarization behavior of HFr and HAc on corrosion of mild steel under the limited test conditions could be possibly due to the difference of temperature dependence of their diffusion coefficients, their pK_a values, or a potential inaccuracy in the temperature function available for K_{HFr} . These speculations prompt the need for further investigation.
- An electrochemical model built to capture the observed behavior has proven to be reasonable accurate at room temperature (at 30 °C), but requires further improvements for higher temperatures.
- While comparing the HFr experimental results with a newly developed mechanistic model, a deviation was observed between the

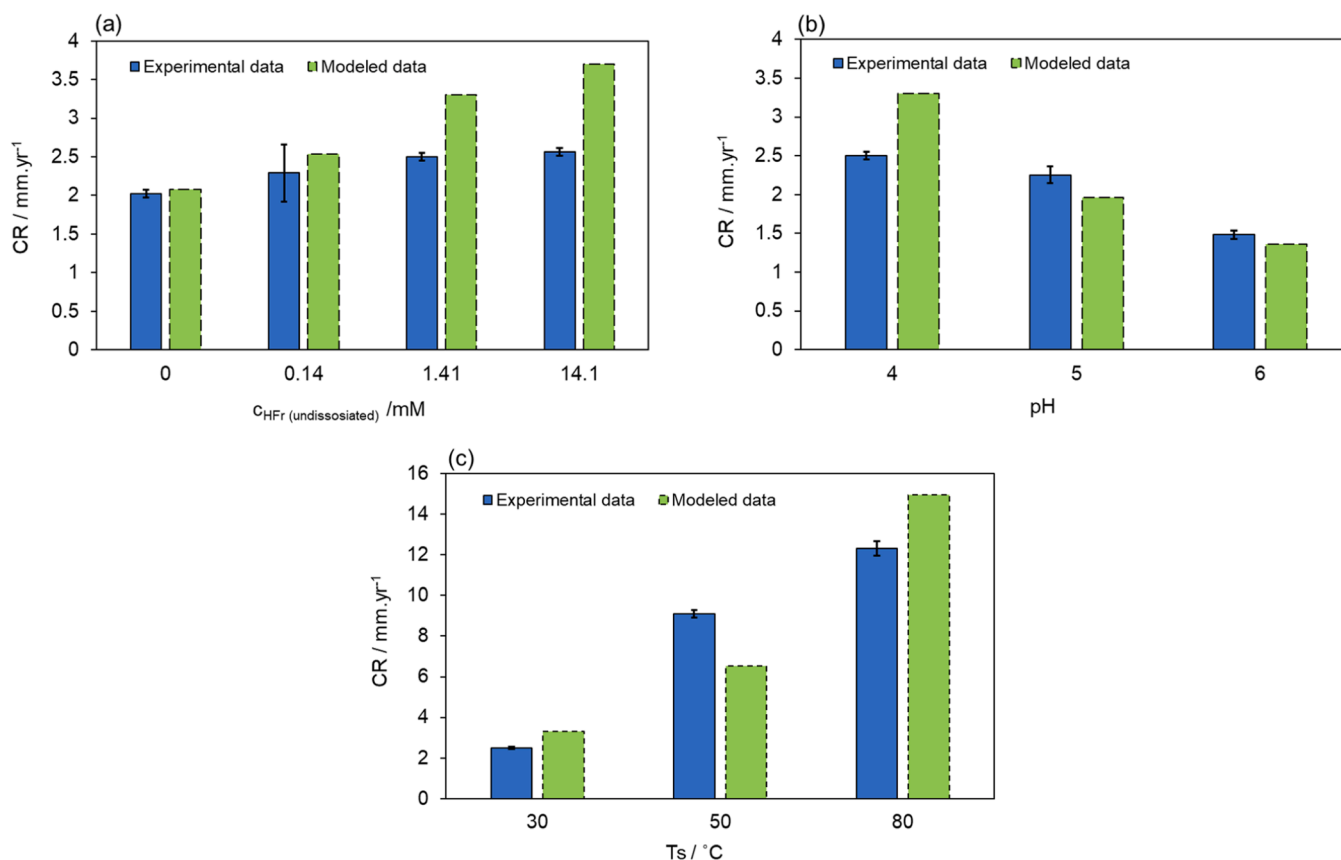


Fig. 19. Comparison between experimental and calculated corrosion rates of X65 steel in N_2 -sparged 1 wt% NaCl solution at 2000 rpm RDE (a) the effect of undissociated HFr concentrations at 30 °C and pH 4, (b) the effect of solution pH at 1.41 mM undissociated HFr and 30 °C, and (c) the effect of temperature at 1.41 mM undissociated HFr and pH 4 (error bars show minimum and maximum values of corrosion rate).

experimental and modeled data in terms of limiting current density, particularly at higher temperatures. It can be speculated that this is a result of possible inaccuracy in the available temperature function for equilibrium constant of HFr dissociation reaction.

CRedit authorship contribution statement

Sahithi Ayyagari: Writing – review & editing, Writing – original draft, Validation, Methodology, Investigation, Formal analysis, Data curation. **Maryam Eslami:** Writing – review & editing, Writing – original draft, Formal analysis, Data curation, Conceptualization. **Fazlollah Madani Sani:** Writing – review & editing, Validation, Formal analysis. **Yoon-Seok Choi:** Writing – review & editing, Validation, Conceptualization. **Bruce Brown:** Writing – review & editing, Project administration. **Srdjan Nestic:** Writing – review & editing, Supervision, Funding acquisition, Conceptualization.

Declaration of competing interest

The authors declare that they have no known competing financial interests or personal relationships that could have appeared to influence the work reported in this paper.

Data availability

Data will be made available on request.

Acknowledgements

The authors would like to thank the following companies for their financial support: Ansys, Baker Hughes, BP, Chevron, Clariant Corporation, ConocoPhillips, M-I SWACO (Schlumberger), Multi-Chem (Halliburton), Occidental Oil Company, Pertamina, Saudi Aramco, Shell Global Solutions, and TOTALenergies.

References

- [1] J. Amri, E. Gulbrandsen, R.P. Nogueira, Pit growth and stifling on carbon steel in CO_2 -containing media in the presence of HAC, *Electrochim. Acta* 54 (2009) 7338–7344.
- [2] J.L. Crolet, M.R. Bonis, Why so low free acetic acid thresholds in sweet corrosion at low PCO_2 ? *Corrosion* (2005). NACE International, Houston, TX Paper No. 05272.
- [3] J.A. Dougherty, A review of the effect of organic acids on CO_2 corrosion, *Corrosion* (2004). NACE International, New Orleans, LA Paper No. 04376.
- [4] E. Gulbrandsen, Acetic acid and carbon dioxide corrosion of carbon steel covered with iron carbonate, *Corrosion* (2007). NACE International Paper No. 07322.
- [5] V. Fajardo, M. Eslami, Y.S. Choi, B. Brown, S. Nestic, Influence of acetic acid on the integrity and protectiveness by an iron carbonate ($FeCO_3$) corrosion product layer, *Corrosion* 77 (2021) 97–111.
- [6] T. Hurlen, S. Gunvaldsen, F. Blaker, Effects of buffers on hydrogen evolution at iron electrodes, *Electrochim. Acta* 29 (1984) 1163–1164.
- [7] Y. Garsany, D. Pletcher, B. Hedges, The role of acetate in CO_2 corrosion of carbon steel: has the chemistry been forgotten? *Corrosion* (2002). NACE International, Denver, CO Paper No. 02273.
- [8] K. George, S. Nestic, C.D. Waard, Electrochemical investigation and modeling of carbon dioxide corrosion of carbon steel in the presence of acetic acid, *Corrosion* (2004). NACE International, New Orleans, LA Paper No. 04379.
- [9] K.S. George, S. Nešić, Investigation of carbon dioxide corrosion of mild steel in the presence of acetic acid—Part 1: basic mechanisms, *Corrosion* 63 (2007) 178–186.
- [10] P.C. Okafor, B. Brown, S. Nestic, CO_2 corrosion of carbon steel in the presence of acetic acid at higher temperatures, *J. Appl. Electrochem.* 39 (2009) 873–877.
- [11] J. Amri, E. Gulbrandsen, R.P. Nogueira, Propagation and arrest of localized attacks in carbon dioxide corrosion of carbon steel in the presence of acetic acid, *Corrosion* 66 (2010) 035001–035007.

- [12] T. Tran, B. Brown, S. Nestic, B. Tribollet, Investigation of the electrochemical mechanisms for acetic acid corrosion of mild steel, *Corrosion* 70 (2014) 223–229.
- [13] A. Kahyarian, B. Brown, S. Nešić, Mechanism of cathodic reactions in acetic acid corrosion of iron and mild steel, *Corrosion* 72 (2016) 1539–1546.
- [14] A. Kahyarian, A. Schumaker, B. Brown, S. Nestic, Acidic corrosion of mild steel in the presence of acetic acid: mechanism and prediction, *Electrochim. Acta* 258 (2017) 639–652.
- [15] E. Gulbrandsen, K. Bilkova, Solution chemistry effects on corrosion of carbon steels in presence of CO₂ and acetic acid, *Corrosion* (2006). NACE International, San Diego, CAPaper No. 06364.
- [16] J.L. Crolet, N. Thevenot, A. Dugstad, Role of Free Acetic Acid On the CO₂ Corrosion of steels, *Corrosion* (1999). NACE International, San Antonio, TXPaper No. 99024.
- [17] J. Amri, E. Gulbrandsen, R.P. Nogueira, Role of acetic acid in CO₂ top of the line corrosion of carbon steel, *Corrosion* (2011). NACE International, Houston, TXPaper No. 11329.
- [18] M.H. Kim, C.S. Kim, H.W. Lee, K. Kim, Temperature dependence of dissociation constants for formic acid and 2,6-dinitrophenol in aqueous solutions up to 175°C, *J. Chem. Soc. Faraday Trans.* 92 (1996) 4951–4956.
- [19] H.S. Harned, R.W. Ehlers, The dissociation constant of acetic acid from 0 to 60°C Centigrade, *J. Am. Chem. Soc.* 55 (1933) 652–656.
- [20] M.M. Singh, A. Gupta, Corrosion behaviour of mild steel in formic acid solutions, *Mater. Chem. Phys.* 46 (1996) 15–22.
- [21] S.K. Singh, A.K. Mukherjee, M.M. Singh, Kinetics of mild steel corrosion in aqueous formic acid solutions, *Can. Metall. Q.* 50 (2011) 186–194.
- [22] S.K. Singh, A.K. Mukherjee, M.M. Singh, Corrosion characteristics of mild steel in aqueous solution of formic acid containing some acetic acid, *Ind. J. Chem. Technol.* 15 (2008) 174–179.
- [23] M. Eslami, Y.S. Choi, S. Nestic, R. Breining, Effect of formic acid (HCOOH) on the corrosion protectiveness of magnetite (Fe₃O₄) at elevated temperature, *Corros. Sci.* 229 (2024) 111868.
- [24] V. Fajardo, C. Canto, B. Brown, S. Nestic, Effect of organic acids in CO₂ corrosion, *Corrosion* (2007). NACE International, Nashville, TNPaper No. 07319.
- [25] S. Nestic, F. Madani Sani, Calculation of cathodic limiting current density in weak acids: part I. aqueous CO₂ solutions, *J. Electrochem. Soc.* 170 (2023) 011504.
- [26] A. Kahyarian, Mechanism and prediction of mild steel corrosion in aqueous solutions containing carboxylic acids, carbon dioxide, and hydrogen sulfide, *Chem. Biomol. Eng.* (2018).
- [27] V.G. Levich, The theory of concentration overpotential, *Acta Physicochim. URSS* 17 (1942).
- [28] J.O.M. Bockris, D. Drazic, A.R. Despic, The electrode kinetics of the deposition and dissolution of iron, *Electrochim. Acta* 4 (1961) 325–361.
- [29] A. Kahyarian, B. Brown, S. Nestic, Electrochemistry of CO₂ corrosion of mild steel: effect of CO₂ on iron dissolution reaction, *Corros. Sci.* 129 (2017) 146–151.
- [30] A. Kahyarian, S. Nestic, A new narrative for CO₂ corrosion of mild steel, *J. Electrochem. Soc.* 166 (2019) C3048.
- [31] S. Ayyagari, M. Eslami, B. Brown, S. Nestic, Corrosion mechanisms of mild steel in the presence of formic acid and acetic acid, in: *Proceedings of the AMPP Annual Conference+ Expo*, San Antonio, TX, 2022. Paper No. 17944.
- [32] Y. Kanzaki, K. Tokuda, S. Bruckenstein, Dissociation rates of weak acids using sinusoidal hydrodynamic modulated rotating disk electrode employing Koutecky-Levich equation, *J. Electrochem. Soc.* 161 (2014) H770.
- [33] W.M. Haynes, *CRC Handbook of Chemistry and Physics*, CRC Press, 2009.
- [34] Y. Kharaka, W. Gunter, P. Aggarwal, E. Perkins, J. DeBaal, A computer program for geochemical modeling of water-rock interactions, *US Geol. Surv. Water-Resour. Investig. Rep.* (1988) 88–4227.
- [35] K. Sue, T. Usami, K. Arai, Determination of acetic acid dissociation constants to 400°C and 32 MPa by potentiometric pH measurements, *J. Chem. Eng. Data* 48 (2003) 1081–1084.
- [36] F.M. Sani, The Effect of Salt Concentration on Aqueous Strong Acid, Carbon Dioxide, and Hydrogen Sulfide Corrosion of Carbon Steel, Ohio University, 2021.
- [37] S. Nestic, J. Postlethwaite, S. Olsen, An electrochemical model for prediction of corrosion of mild steel in aqueous carbon dioxide solutions, *Corrosion* 52 (1996) 280–294.
- [38] M. Nordsveen, S. Nešić, R. Nyborg, A. Stangeland, A mechanistic model for carbon dioxide corrosion of mild steel in the presence of protective iron carbonate films—Part 1: theory and verification, *Corrosion* 59 (2003) 443–456.
- [39] R.R. Dogonadze, Application of rotating disc electrode to study kinetic and catalytic processes in electrochemistry: a case of different diffusion coefficients, *Russ. J. Phys. Chem. A* 27 (1958) 2437–2442.
- [40] F. Madani Sani, S. Nestic, A critical review of models for density, viscosity, and diffusivity in aqueous sodium chloride solutions, *Electrochim. Acta* 477 (2024) 143766.
- [41] M.L. Batzle, Z. Wang, Seismic properties of pore fluids, *Geophysics* 57 (1992) 1396–1408.
- [42] S. Mao, Z. Duan, The viscosity of aqueous alkali-chloride solutions up to 623 K, 1,000 bar, and high ionic strength, *Int. J. Thermophys.* 30 (2009) 1510–1523.
- [43] C.A.J. Appelo, Solute transport solved with the Nernst-Planck equation for concrete pores with ‘free’ water and a double layer, *Cem. Concr. Res.* 101 (2017) 102–113.
- [44] M. Ciszowska, Z. Stojek, S.E. Morris, J.G. Osteryoung, Steady-state voltammetry of strong and weak acids with and without supporting electrolyte, *Anal. Chem.* 64 (1992) 2372–2377.
- [45] M.B. Hariri, B. Brown, S. Nestic, Kinetics of iron dissolution: a new approach for modeling the anodic potentiodynamics based on transient analysis, in: *Proceedings of the AMPP Annual Conference+Expo*, Denver, CO, 2023. Paper No. 19073.